BULLETIN OF THE POLISH ACADEMY OF SCIENCES
TECHNICAL SCIENCES, Vol. 72(1), 2024, Article number: e147926
DOI: 10.24425/bpasts.2023.147926

SPECIAL SECTION

Comparative study of experimental thermographic data and finite element analysis on temperature evolution of PET-G layer deposition during additive manufacturing process

Łukasz KOWALSKI[1], **Michał Bembenek**[1]*, **Andrzej Uhryński**[2], **and Szymon Bajda**[3]

[1] Department of Manufacturing Systems, Faculty of Mechanical Engineering and Robotics, AGH University of Krakow, Al. Adama Mickiewicza 30, 30-059 Kraków, Poland
[2] Department of Machine Design and Maintenance, Faculty of Mechanical Engineering and Robotics, AGH University of Krakow, Al. Adama Mickiewicza 30, 30-059 Kraków, Poland
[3] Faculty of Metals Engineering and Industrial Computer Science, AGH University of Krakow, Al. Adama Mickiewicza 30, 30-059, Kraków, Poland

Abstract. Additive manufacturing (AM) technologies have been gaining popularity in recent years due to patent releases – and in effect – better accessibility of the technology. One of the most popular AM technologies is fused deposition modeling (FDM), which is used to manufacture products out of thermoplastic polymers in a layer-by-layer manner. Due to the specificity of the method, parts manufactured in this manner tend to have non-isotropic properties. One of the factors influencing the part's mechanical behavior and quality is the thermoplastic material's bonding mechanism correlated with the processing temperature, as well as thermal shrinkage during processing. In this research, the authors verified the suitability of finite element method (FEM) analysis for determining PET-G thermal evolution during the process, by creating a layer transient heat transfer model, and comparing the obtained modelling results with ones registered during a real-time process recorded with a FLIR T1020 thermal imaging camera. Our model is a valuable resource for providing thermal conditions in existing numerical models that connect heat transfer, mesostructure and AM product strength, especially when experimental data is lacking. The FE model presented reached a maximum sample-specific error of 11.3%, while the arithmetic mean percentage error for all samples and layer heights is equal to 4.3%, which the authors consider satisfactory. Model-to-experiment error is partially caused by glass transition of the material, which can be observed on the experimental cooling rate curve after processing the temperature signal.

Keywords: FDM; 3D printing; thermography; FEA.

1. INTRODUCTION

Additive manufacturing (AM) is a group of manufacturing technologies for which the manufacturing process is done through adding material to a part until its desired shape is achieved. Since C.W. Hull patented his stereolithography apparatus [1], many new AM methods, also known as 3D printing methods, were developed. ISO/ASTM standard 52900:2015 [2] defines 7 major groups of 3D printing technologies: binder jetting, directed energy deposition, material extrusion, material jetting, powder bed fusion, sheet lamination and vat photopolymerization [3].

In the material extrusion group, there is a method called fused deposition modeling (FDM) which allows manufacturing of products out of various thermoplastic polymeric materials and their composites, adding a material in a layer-by-layer manner [4]. The materials commonly used in 3D printing include polylactic acid (PLA), acrylonitrile-butadiene-styrene (ABS), polypropylene (PP), polyethylene-terephthalate glycol-modified (PET-G) and nylon, to name just a few [5, 6].

Because of the layer-by-layer fabrication method and the ability to make complex internal macrostructures, FDM manufactured parts show anisotropic mechanical properties [7]. Those properties are influenced by raw material characteristics, but also by FDM processing parameters such as: spatial orientation during printing [8], shape of the product [9], layer thickness [10], infill pattern and density [11, 12], as well as processing temperature of the envelope, printer's buildplate and extrusion [13–16].

Anisotropy phenomena are also induced by the infill topology in the case of relative density smaller than 1, which can be further compounded by the use of composite fibrous polymeric materials such as short glass fiber reinforced polyamide [17]. Such materials can also be used to supplement printing manufacturing methods different than 3D, for example when preparing a GPET core of sandwich structures reinforced with carbon fibers [18]. Melt flow numerical analysis can be used to design new composite polymeric materials for additive manufacturing, as shown by Mostafa *et al.* [19] on the example of an ABS-iron composite.

For thermoplastic polymers in general, parameters of the final product such as achievability of the desired part geometry can be affected by the material's crystallization mechanisms and cooling rate after processing [20, 21]. In [22], Kuznetsov *et al.* used

*e-mail: bembenek@agh.edu.pl

Manuscript submitted 2023-01-04, revised 2023-10-03, initially accepted for publication 2023-10-30, published in February 2024.

© 2024 The Author(s). This is an open access article under the CC BY license (http://creativecommons.org/licenses/by/4.0/)

thermographic data to determine the influence of temperature flow on the strength of PLA samples in a three-point bending test, formulating a method to calculate ultimate fracture strength with the aid of measured sub-layer temperature.

In terms of FDM technology, those parameters can be controlled indirectly by using a printer with a closed and heated chamber, using a cooling fan and adjusting temperature of the buildplate and the extruder hotend. Studies show that proper control over thermal processing parameters can help in obtaining better contact interface between layers and lines of a printed polymer [22–24], which leads to increased strength of the final product. Better dimensional accuracy and a successful printing process can also be achieved by adjusting the buildplate temperature [25] or the cooling rate [26]. Temperature analysis was also used to help determine new infill structures for 3D prints that increase process dimensional accuracy [27,28]. Process temperature can also affect crystallization mechanisms, and in effect influence impact strength and bonding strength of manufactured parts [29, 30]. To simulate thermodynamic processes in FDM and their correlations to various material parameters, complex numerical and analytical models are created [31].

Recently, Karimnejad et al. improved preexisting mathematical models of the bond forming in FDM, allowing to determine neck size between neighboring filament lines, correlating mesostructure of the material with temperature flow during processing, allowing in effect to determine the product's strength properties [32]. The rheological behavior of extruded AM PLA was analyzed by Mackay [33, 34], showing the importance of heat transfer within the processing system and the manufactured part and its influence on the product's quality and strength.

Thermography or thermal imaging is a method during which the infrared radiation of an object is captured using a thermal camera. It's a method that has found many applications – in assessment of buildings' thermal insulation [35], medical diagnostics [36], manufacturing process analysis [37] or industrial tools diagnostics and process control [38]. Thermography can also be used for FDM process control and analysis – determining the formation of welding zones between polymeric material layers [39] or analyzing non-standard 3D printing methods such as big area additive manufacturing [40], where due to the scale, thermodynamical processes play a larger role. Thermal imaging can also be used for diagnostics and failure prediction of previously AM parts [41].

Due to the visible influence of temperature during processing on AM product's mechanical properties [6], as well as the applicability of the material's thermal evolution during the deposition process on mesostructure and strength properties modelling [31, 42], in this research the authors decided to develop a numerical model of temperature evolution during FDM printing. The capacity to conduct FEA analysis for determining thermal conditions, including cooling rates of specific layers during the FDM process, is crucial. Our model is a valuable tool for providing thermal conditions for current numerical models that establish relationships between heat flow, mesostructure and the strength of AM products, especially in the cases where experimental data are limited or unavailable. Thermographic data were used to validate the model.

2. MATERIALS AND METHODS

The material chosen by the authors to carry out the research was white "Easy PET-G" (Fiberlab S.A., Brzezie, Poland) due to this material's broad applicability in 3D printing and availability in the local market. Some of the material's thermal and mechanical parameters provided by the manufacturer are presented in Table 1.

Table 1
Selected properties of easy PET-G, per manufacturer's data [43]

Tensile strength, in MPa	Yield point, in MPa	Tensile modulus, in MPa	Elongation at break, in %	Glass transition temperature, in °C
51	51	2800	29	82

Some of the material parameters required to properly model its thermal behavior were not covered by the data provided by the manufacturer, so the authors used average values of matweb data for PET-G instead (Table 2). To enhance the accuracy of the model, it is worth noting that future research could consider obtaining these data through empirical experimentation rather than relying on estimated data sourced from the literature.

Table 2
Selected properties of the examined material used in this research [44]

Specific heat capacity, in J/g°C	Thermal conductivity, in W/mK	Glass transition temperature, in °C	Decomposition temperature, in °C
1.10–1.30	0.162–0.225	79–85	70–280

Emissivity of the samples was determined experimentally using a Teledyne FLIR T1020 HD thermal camera (Wilsonville, USA). The samples were placed on a hot plate alongside the reference material with known emissivity of 0.95. Afterwards, after adjusting the values of room temperature and air humidity in the FLIR camera settings, the plate with the samples was preheated to 120°C and left for cooling. Then a thermographic photo was taken for each 1°C temperature decrease until the reference material reached room temperature. Photographs were taken with a camera mounted on a tripod, perpendicularly to the photographed surface with the reference placed in the center of the photos. Using FLIR Studio software (Teledyne FLIR, Wilsonville, USA) the images thus acquired were analyzed by adjusting the emissivity values so the temperature reading on the sample's surface matched the reading on the reference material. Using this method, the authors obtained the emissivity of 3D printed PET-G equal to 0.88. The method is presented in the photos (Fig. 1) for clarification purposes. Before the experiment the material was dried in the oven at 65°C for 5 hours.

To measure the temperature change during the FDM 3D printing process, the authors designed a sample that allows to be observed for a suitable period of time while the process conditions

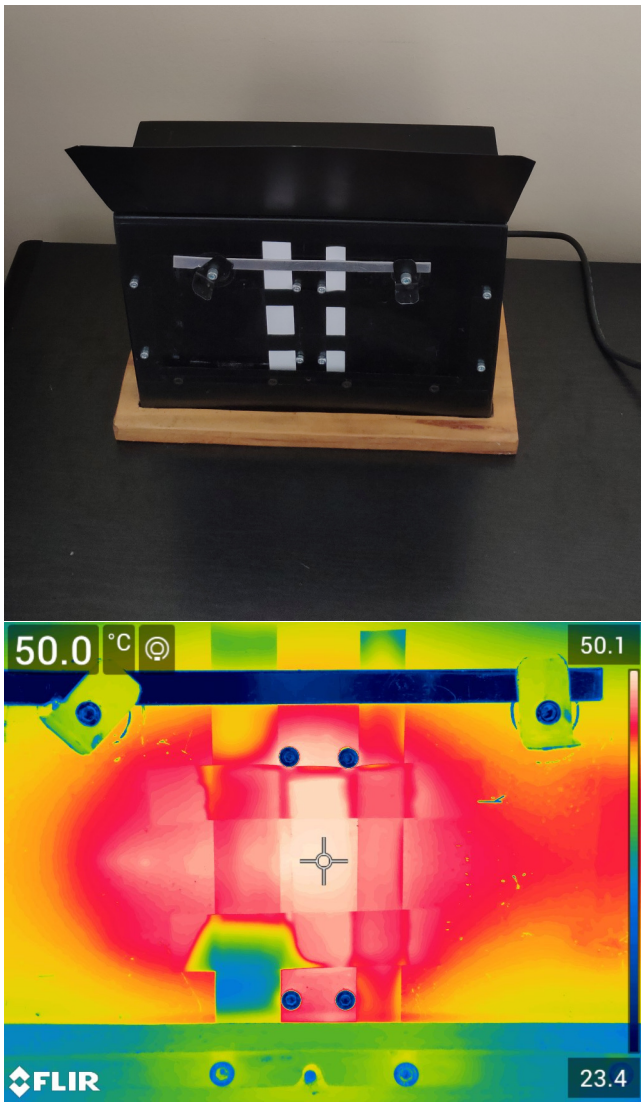

Fig. 1. Samples mounted on a hot plate (white material, top side) and thermographic image taken for determining the emissivity of the sample (bottom side)

(specifically printer head displacement speed and material feedrate) remain constant and the heat exchange process between freshly laid material occurs only between the air enveloping it and previously laid material layers.

The designed sample was processed using Simplify 3D software (Simplify3D, Cincinnati, USA) to generate a g-code file for the 3D printer. Printing parameters for the process are presented in Table 3. Three different g-codes were prepared for layer heights of 0.20, 0.24 and 0.28 mm, with the remaining process parameters being constant. The specimen is designed to be printed in "vase mode", so no retractions occur during the whole process, and the printhead always moves in one direction, without idle movements. The straight line, 200 mm in length (Fig. 2), was the zone analyzed in this research.

Table 3
FDM 3D printing process parameters for the experiment

Printing temperature, in °C	Heated bed temperature, in °C	Printing speed, in mm/s	Layer height, in mm	Layer width, in mm
232	80	35	0.20; 0.24; 0.28	0.48

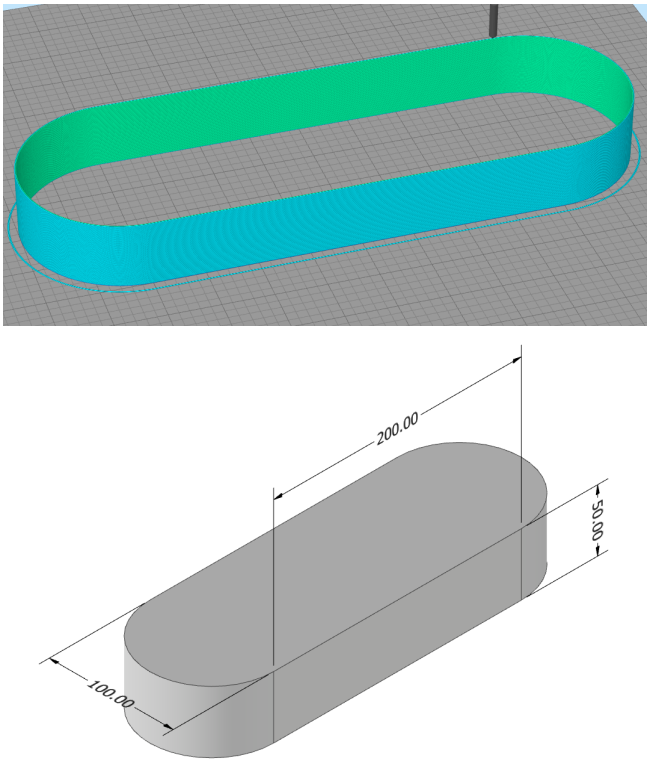

Fig. 2. Sample for process analysis with dimensions in mm (bottom side), and 3D print preview from Simplify 3D software (top side)

The experiment was conducted using an Anycubic Chiron 3D printer (Shenzhen Anycubic Technology, Shenzhen, China), in a windowless room without any additional heat sources, and with the lights turned off during measurements. The standard hotend nozzle was used (0.4 mm). The machine was maintained in optimal and original working conditions during the experimentation period. The heated bed was leveled using the automatic multi-point leveling method, with a mechanical probe. Before starting the process, air humidity and room temperature were measured, being respectively 50% and 23°C. The temperature measurement coincided with the readings on the 3D printer's heatbed and hotend thermistors. Throughout the experiment, air humidity and temperature were monitored and remained the same.

The FLIR camera was placed on a tripod, with the distance between the observed surface and the camera lens being 300 mm. The first few processes observed through the camera were not recorded, but used to determine if there are any infrared reflections from the environment that could influence the measurement, which would need to be eliminated before obtaining thermal data for analysis. Afterwards, for each layer height, a 1280×960 resolution thermographic video was recorded.

In total, 15 thermographic videos were recorded (Table 4) for assessing how the distance from the printer's heatbed affects the new layer's temperature evolution, including three 5-minute recordings at a print height above 15 mm for finite element model verification. The video framerate allowed to obtain layer temperature samples every 0.033 seconds.

Table 4
Thermographic data collection, recordings list

Layer height, in mm	Moment of recording (print height at the start of observation), in mm	Video length
0.20, 0.24, 0.28	2	Until 2 new layers are printed
	7	
	15	
	20	
	15	5 minutes

Measurements from each video were taken manually with the measurement starting point located under the hotend nozzle when the hotend is located in the middle area of the picture. Then for each subsequent frame the temperature value was recorded to create a cooling curve for the material. The location of the said starting point is visualized in Fig. 3, along with indicative frame dimensions. To validate the experimental data at set distances between the heatbed and the currently applied layer of the material, the cooling data were recorded at different nozzle locations as a starting point into a comma separated values file (.csv), displaying insignificant variations.

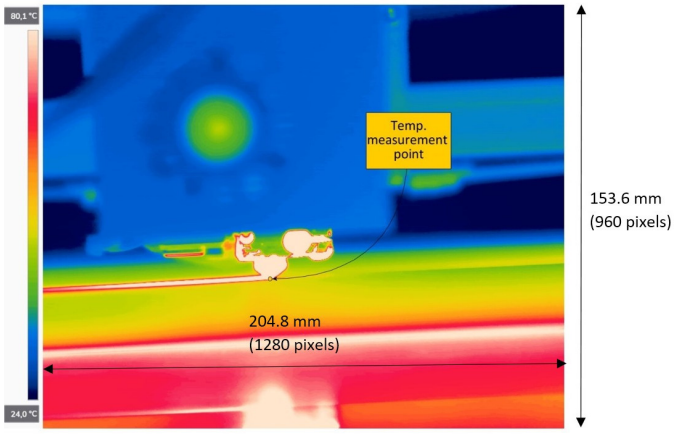

Fig. 3. Location of temperature measurement point

After collecting the data, a numerical model was created for the Abaqus Standard solver (Dassault Systèmes SE, Vélizy-Villacoublay, France). The parts of the model were created using 8-node linear heat transfer brick element types (DC3D8). The DC3D8 element is a three-dimensional, solid element commonly used for modeling complex geometries and analyzing thermal behavior. It is suitable for simulating heat transfer and provides a high degree of accuracy in capturing temperature gradients within the material. The model geometry is presented schematically in Fig. 4 (left side). For process simplification and in order to shorten calculation time, only a fraction of the full model is used. The length of the analyzed layer is 5 mm, and previous layers are modelled as a homogenous block with height equal to 15 mm. Material for layers was defined using parameters from Tables 1 and 2. The heatbed was modelled as a fixed glass piece, 2.8 mm thick, with its body temperature equal to constant 80°C. The material's deposition process was simulated using a subroutine, laying new 0.1 mm long segments at an initial temperature of 232°C. Printing speed was set to 35 mm/s, and this process continued until a complete 5 mm-long layer was formed (Fig. 4, right side). Ambient temperature was set to 23°C. During the initial experimental observations, it was noted that depositing a new layer of material during printing above 10 mm of print height creates a vertical temperature gradient within 1 mm of topside layers, which stabilizes below that at about ½of heatbed temperature (40°C in the case being analyzed). Said gradient was implemented in the model and is visible in Fig. 4 as well. The heat exchange process was modelled within the timeframe from 0 to 4 seconds, divided into equally long samples of 0.033 seconds, so the sampling in the experiment matches with the model sampling rate.

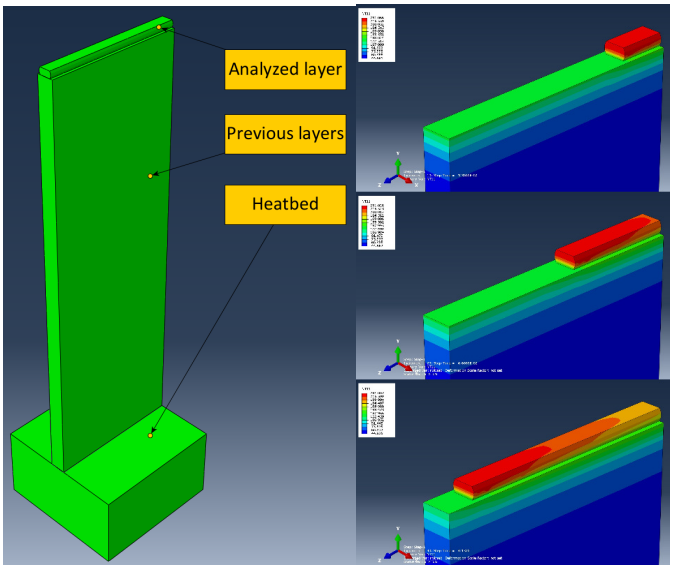

Fig. 4. FEA block model (left side) and principle of material deposition (right side)

The modeled layer's cross section geometry and dimensions are presented in Fig. 5. The value of h in the drawing is a variable representing the modelled layer height. We considered three different layer height values: 0.2, 0.24 and 0.28 mm, while the width remained constant at 0.48 mm. The remaining dimensions result from the parameters set during g-code preparation.

The temperature samples from the model were recorded in a manner similar to the experimental measurements, i.e. from

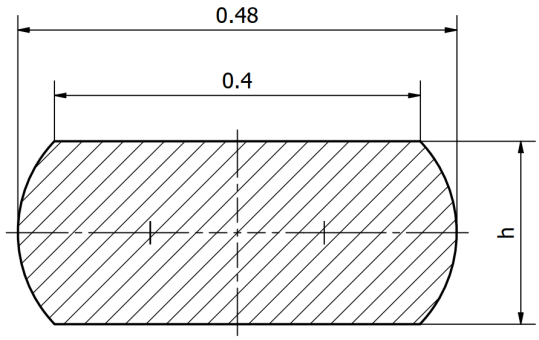

Fig. 5. Shape and dimensions of the layer cross-section

the element placed in the middle of the extrusion line. To adjust values obtained from the real measurement with values from the model for comparative purposes, and to eliminate potential influence of hotend nozzle's proximity on the first few samples, the moment at which both datasets begin (initial time $t_0 = 0$ seconds) is the moment when temperature sample value is the closest to 200°C, and then the readings are continued until $t = 3$ seconds. To represent the deviation between calculated and measured data, the following formula was used:

$$T_D = \frac{\sum_{i=1}^{n} (T_{\mathrm{ex}_i} - T_{\mathrm{mod}_i})}{n}, \tag{1}$$

where T_{ex_i} and T_{mod_i} are the i-sample of experimental temperature and model temperature, respectively, in °C. The following formula was used to represent the rate of temperature change:

$$\Delta T\,(T_{n+1}, t_{n+1}) = \frac{T_n - T_{n+1}}{t_{n+1} - t_n}, \tag{2}$$

where $\Delta T(t)$ is the cooling rate function (in °C/s) and t_{n+1} is a time at which the T_{n+1} sample was recorded. For readability of the experimental data, the $\Delta T\,(T_{n+1}, t)$ function was smoothed using simple moving average (SMA), as per the following formula:

$$\Delta T_{\mathrm{SMA}}(t_{n+8}) = \frac{\sum_{i=1}^{8} (\Delta T\,(T_{i+1}, t))}{8}, \tag{3}$$

where t_n is the time at which sample n is registered and 8 is the SMA period which represents a timeframe of 0.263 second.

3. RESULTS AND DISCUSSION

We conducted a mesh sensitivity analysis by systematically refining the mesh to assess its impact on our results and to determine optimal mesh density for stability and accuracy (Fig. 6). Various element sizes were considered, including 0.2, 0.1, 0.05 and 0.025. Notably, the use of the largest element size (0.2) resulted in noticeably different results as compared to the other sizes, which exhibited similar outcomes. Consequently, we selected an element size of 0.1 for the analysis. This choice balances high accuracy in results with relatively efficient simulation times.

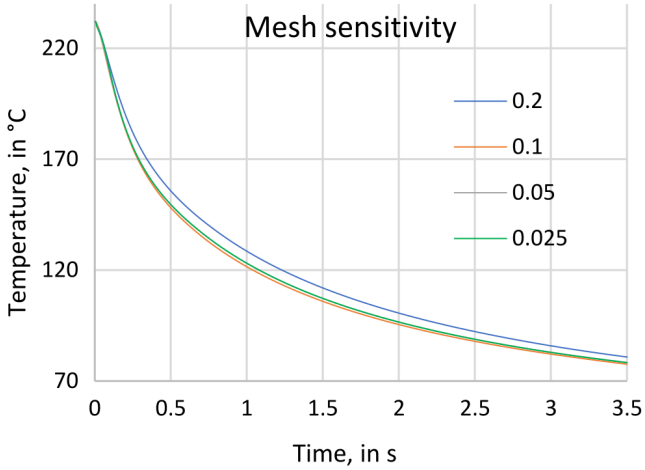

Fig. 6. Mesh sensitivity analysis for various element sizes: 0.2, 0.1, 0.05 and 0.025

A comparison of the modelling results with the experimental results for the temperature evolution within the extruded 3D printing layer from the moment of extrusion (at $t = 0$) is represented in the graphs (Fig. 7) for the different layer heights analyzed. The mean deviation between modelling and experimental results calculated by formula (1) for the timeframe between 0 and 3 seconds is the largest for layer height of 0.28 mm (LH028), being 4.95°C. The largest overall model flat error can also be observed for LH028, being 10.3°C at $T_{\mathrm{ex}} = 121.3$°C (8.5%). The model for LH028 has a tendency to underestimate the temperature value (91% of samples below real temperature), quite oppositely to the model for the layer height of 0.20 mm (LH020), where 100% of the samples are overestimated, while the model for the layer height of 0.24 mm (LH024) can be placed in the middle (50% of over- and underestimated samples). Because of that, FE model for LH024 has the smallest mean error of −0.64°C and the maximum error of 4.7°C at $T_{\mathrm{ex}} = 106.1$°C (4.4%). Maximum model flat error for LH020 was −8.6°C, observed at $T_{\mathrm{ex}} = 76.1$°C (11.3%).

By observing graphs representing material cooling rates (Fig. 8) calculated using formulas (2) and (3), it is visible that at the end of the cooling process, the cooling speed starts accelerating at about $T_{\mathrm{ex}} = 110$°C for each layer height, reaching the local maximum at 106.2°C (for LH020), 94.7°C (for LH024) and 106.5°C (for LH028), respectively. The phenomenon might be caused by phase transition initiation, as the sources indicate the glass transition temperature of PET-G stands at about 79–85°C (Table 2).

The SMA of the cooling rate seems to be visibly slower in experimental data at initial cooling stages only for LH028 (19.5%). For LH024 the initial model cooling rate is only 0.5% smaller than the experimental one, and for LH020 it's 8.6% larger.

Detailed data about the percentage model error for each sample is presented in Fig. 9. It can be concluded that the presented

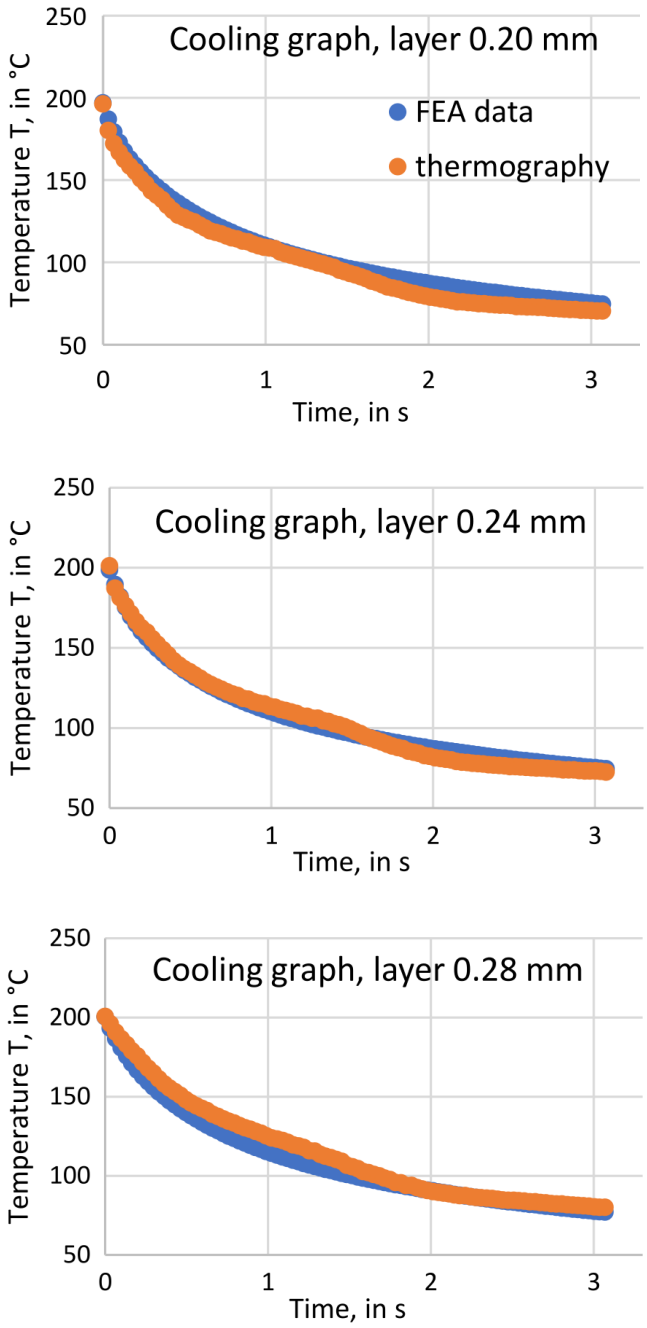

Fig. 7. Comparison of temperature change measured in the experiment and calculated by the model for different layer heights

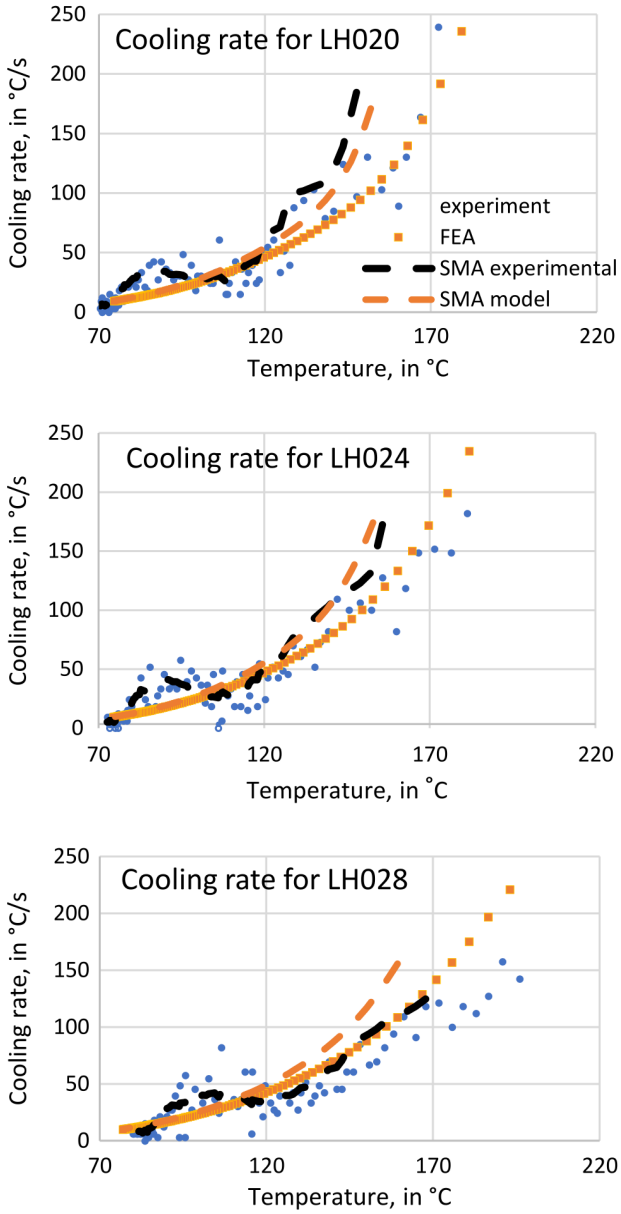

Fig. 8. Cooling rates for experimental and FEA data

FE model can be used to predict PET-G layer temperature evolution during the FDM 3D printing process with a maximum error of 11.3% for lower temperature ranges of the LH020 model. Arithmetic mean percentage error for all the samples and layer heights is equal to 4.3%, which can be considered satisfactory. Model accuracy could be improved by using thermal data such as the convective film coefficient and specific heat capacity of the material obtained empirically instead of using estimated data from the literature. The model could be enhanced further by determining how the beforementioned parameters change in correlation to temperature.

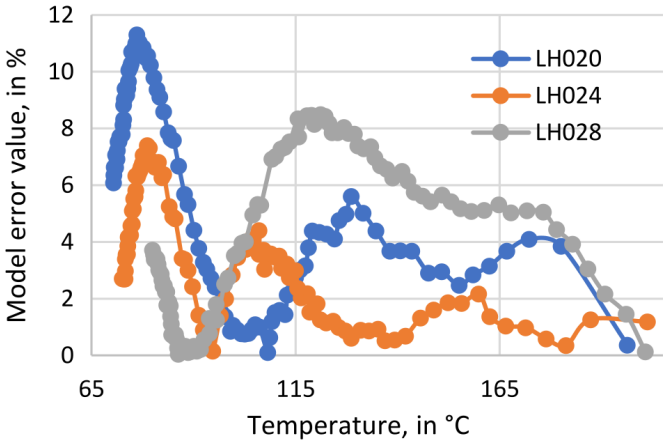

Fig. 9. Percentage error for each sample, model data compared to experimental data

ACKNOWLEDGEMENTS

This research was supported in part by PLGrid Infrastructure.

REFERENCES

[1] C.W. Hull, "Apparatus for production of three-dimensional objects by stereolithography," U.S. Patent US4575330A, Mar. 11, 1986 Accessed: Jul. 14, 2022. [Online]. Available: https://patents.google.com/patent/US4575330A/en?inventor=charles+w.+hull&oq=charles+w.+hull&sort=old&page=1

[2] ISO/ASTM, "ISO/ASTM 52900:2015 Additive manufacturing – General principles – Fundamentals and vocabulary," *International Organization for Standardization ISO*.

[3] S.A.M. Tofail, E.P. Koumoulos, A. Bandyopadhyay, S. Bose, L. O'Donoghue, and C. Charitidis, "Additive manufacturing: scientific and technological challenges, market uptake and opportunities," *Mater. Today*, vol. 21, no. 1, pp. 22–37, Jan. 2018, doi: 10.1016/j.mattod.2017.07.001.

[4] R. Patel, C. Desai, S. Kushwah, and M.H. Mangrola, "A review article on FDM process parameters in 3D printing for composite materials," *Mater. Today Proc.*, vol. 60, pp. 2162–2166, Jan. 2022, doi: 10.1016/j.matpr.2022.02.385.

[5] A. Sharma and A. Rai, "Fused deposition modelling (FDM) based 3D & 4D Printing: A state of art review," *Mater. Today Proc.*, vol. 62, pp. 367–372, 2022, doi: 10.1016/j.matpr.2022.03.679.

[6] M. Bembenek, Ł. Kowalski, and A. Kosoń-Schab, "Research on the Influence of Processing Parameters on the Specific Tensile Strength of FDM Additive Manufactured PET-G and PLA Materials," *Polymers*, vol. 14, no. 12, p. 2446, Jan. 2022, doi: 10.3390/polym14122446.

[7] Md. Qamar Tanveer, G. Mishra, S. Mishra, and R. Sharma, "Effect of infill pattern and infill density on mechanical behaviour of FDM 3D printed Parts – a current review," *Mater. Today Proc.*, vol. 62, pp. 100–108, Jan. 2022, doi: 10.1016/j.matpr.2022.02.310.

[8] S. Farashi and F. Vafaee, "Effect of printing parameters on the tensile strength of FDM 3D samples: a meta-analysis focusing on layer thickness and sample orientation," *Prog. Addit. Manuf.*, vol. 7, pp. 565–582, Jan. 2022, doi: 10.1007/s40964-021-00247-6.

[9] M. Bembenek, Ł. Kowalski, J. Pawlik, and S. Bajda, "Research on the Influence of the Load Direction and the Cross-Section Shape on the Young's Modulus of Elements Produced by the Fused Deposition Modeling Method," *J. Mater. Eng. Perform.*, vol. 31, pp. 7906–7912, Apr. 2022, doi: 10.1007/s11665-022-06848-8.

[10] M.S. Amirruddin, K.I. Ismail, and T.C. Yap, "Effect of layer thickness and raster angle on the tribological behavior of 3D printed materials," *Mater. Today Proc.*, vol. 48, pp. 1821–1825, Jan. 2022, doi: 10.1016/j.matpr.2021.09.139.

[11] M.T. Birosz, D. Ledenyák, and M. Andó, "Effect of FDM infill patterns on mechanical properties," *Polym. Test.*, vol. 113, p. 107654, Sep. 2022, doi: 10.1016/j.polymertesting.2022.107654.

[12] J. Dobos, M.M. Hanon, and I. Oldal, "Effect of infill density and pattern on the specific load capacity of FDM 3D-printed PLA multi-layer sandwich," *J. Polym. Eng.*, vol. 42, no. 2, pp. 118–128, Feb. 2022, doi: 10.1515/polyeng-2021-0223.

[13] K.M. Agarwal, P. Shubham, D. Bhatia, P. Sharma, H. Vaid, and R. Vajpeyi, "Analyzing the Impact of Print Parameters on Dimensional Variation of ABS specimens printed using Fused Deposition Modelling (FDM)," *Sens. Int.*, vol. 3, p. 100149, Jan. 2022, doi: 10.1016/j.sintl.2021.100149.

[14] M. Grasso, L. Azzouz, P. Ruiz-Hincapie, M. Zarrelli, and G. Ren, "Effect of temperature on the mechanical properties of 3D-printed PLA tensile specimens," *Rapid Prototyp. J.*, vol. 24, no. 8, pp. 1337–1346, Jan. 2018, doi: 10.1108/RPJ-04-2017-0055.

[15] D. Frunzaverde *et al.*, "The Influence of the Printing Temperature and the Filament Color on the Dimensional Accuracy, Tensile Strength, and Friction Performance of FFF-Printed PLA Specimens," *Polymers*, vol. 14, no. 10, p. 1978, Jan. 2022, doi: 10.3390/polym14101978.

[16] V. Cojocaru, D. Frunzaverde, C.-O. Miclosina, and G. Marginean, "The Influence of the Process Parameters on the Mechanical Properties of PLA Specimens Produced by Fused Filament Fabrication – A Review," *Polymers*, vol. 14, no. 5, p. 886, Jan. 2022, doi: 10.3390/polym14050886.

[17] P.J. Lal Lazar, J. Subramanian, E. Natarajan, K. Markandan, and S. Ramesh, "Anisotropic structure-property relations of FDM printed short glass fiber reinforced polyamide TPMS structures under quasi-static compression," *Mater. Res. Technol-JMRT*, vol. 24, pp. 9562–9579, May 2023, doi: 10.1016/j.jmrt.2023.05.167.

[18] J. Andrzejewski, M. Gronikowski, and J. Aniśko, "A Novel Manufacturing Concept of LCP Fiber-Reinforced GPET-Based Sandwich Structures with an FDM 3D-Printed Core," *Materials*, vol. 15, no. 15, p. 5404, Jan. 2022, doi: 10.3390/ma15155405.

[19] N. Mostafa, H.M. Syed, S. Igor, and G. Andrew, "A Study of Melt Flow Analysis of an ABS-Iron Composite in Fused Deposition Modelling Process," *Tsinghua Sci. Technol.*, vol. 14, pp. 29–37, Jun. 2009, doi: 10.1016/S1007-0214(09)70063-X.

[20] S. Han and K.K. Wang, "Shrinkage Prediction for Slowly-Crystallizing Thermoplastic Polymers in Injection Molding," *Int. Polym. Process.*, vol. 12, no. 3, pp. 228–237, Sep. 1997, doi: 10.3139/217.970228.

[21] L. Benedetti, B. Brulé, N. Decreamer, K.E. Evans, and O. Ghita, "Shrinkage behaviour of semi-crystalline polymers in laser sintering: PEKK and PA12," *Mater. Des.*, vol. 181, p. 107906, Nov. 2019, doi: 10.1016/j.matdes.2019.107906.

[22] V.E. Kuznetsov, A.N. Solonin, A. Tavitov, O. Urzhumtsev, and A. Vakulik, "Increasing strength of FFF three-dimensional printed parts by influencing on temperature-related parameters of the process," *Rapid Prototyp. J.*, vol. 26, no. 1, pp. 107–121, Jan. 2020, doi: 10.1108/RPJ-01-2019-0017.

[23] T.E. Shelton, Z.A. Willburn, C.R. Hartsfield, G.R. Cobb, J.T. Cerri, and R.A. Kemnitz, "Effects of thermal process parameters on mechanical interlayer strength for additively manufactured Ultem 9085," *Polym. Test.*, vol. 81, p. 106255, Jan. 2020, doi: 10.1016/j.polymertesting.2019.106255.

[24] Q. Sun, G.M. Rizvi, C.T. Bellehumeur, and P. Gu, "Effect of processing conditions on the bonding quality of FDM polymer filaments," *Rapid Prototyp. J.*, vol. 14, no. 2, pp. 72–80, Mar. 2008, doi: 10.1108/13552540810862028.

[25] Y.-H. Choi, C.-M. Kim, H.-S. Jeong, and J.-H. Youn, "Influence of Bed Temperature on Heat Shrinkage Shape Error in FDM Additive Manufacturing of the ABS-Engineering Plastic," *World J. Eng. Technol.*, vol. 4, no. 3, pp. 186–192, Oct. 2016, doi: 10.4236/wjet.2016.43D022.

[26] M. Faes, E. Ferraris, and D. Moens, "Influence of Inter-layer Cooling time on the Quasi-static Properties of ABS Components Produced via Fused Deposition Modelling," *Procedia CIRP*, vol. 42, pp. 748–753, Jan. 2016, doi: 10.1016/j.procir.2016.02.313.

[27] U.M. Dilberoglu, S. Simsek, and U. Yaman, "Shrinkage compensation approach proposed for ABS material in FDM process," *Mater. Manuf. Process.*, vol. 34, no. 9, pp. 993–998, Jul. 2019, doi: 10.1080/10426914.2019.1594252.

[28] U. Yaman, "Shrinkage compensation of holes via shrinkage of interior structure in FDM process," *Int. J. Adv. Manuf. Technol.*, vol. 94, no. 5–8, pp. 2187–2197, Feb. 2018, doi: 10.1007/s00170-017-1018-2.

[29] C. Benwood, A. Anstey, J. Andrzejewski, M. Misra, and A.K. Mohanty, "Improving the Impact Strength and Heat Resistance of 3D Printed Models: Structure, Property, and Processing Correlationships during Fused Deposition Modeling (FDM) of Poly(Lactic Acid)," *ACS Omega*, vol. 3, no. 4, pp. 4400–4411, Apr. 2018, doi: 10.1021/acsomega.8b00129.

[30] C. Bellehumeur, L. Li, Q. Sun, and P. Gu, "Modeling of Bond Formation Between Polymer Filaments in the Fused Deposition Modeling Process," *J. Manuf. Process.*, vol. 6, no. 2, pp. 170–178, Jan. 2004, doi: 10.1016/S1526-6125(04)70071-7.

[31] S. Garzon-Hernandez, D. Garcia-Gonzalez, A. Jérusalem, and A. Arias, "Design of FDM 3D printed polymers: An experimental-modelling methodology for the prediction of mechanical properties," *Mater. Des.*, vol. 188, p. 108414, Mar. 2020, doi: 10.1016/j.matdes.2019.108414.

[32] A. Karimnejad, Z. Taheri, and A. Ramiar, "Predicting the neck size in the fused filament fabrication process," *Int. J. Adv. Manuf. Technol.*, vol. 126, pp. 67–86, 2023, doi: 10.1007/s00170-023-11039-3.

[33] M.E. Mackay, "The importance of rheological behavior in the additive manufacturing technique material extrusion," Journal of Rheology, vol. 62, no. 6, pp. 1549–1561, Nov. 2018, doi: 10.1122/1.5037687.

[34] M.E. Mackay, Z.R. Swain, C.R. Banbury, D.D. Phan, and D.A. Edwards, "The performance of the hot end in a plasticating 3D printer," *J. Rheol.*, vol. 61, no. 2, p. 229, Jan. 2017, doi: 10.1122/1.4973852.

[35] C.A. Balaras and A.A. Argiriou, "Infrared thermography for building diagnostics," *Energy Build.*, vol. 34, no. 2, pp. 171–183, Feb. 2002, doi: 10.1016/S0378-7788(01)00105-0.

[36] J.H.L. Branco, R.L.L. Branco, T.C. Siqueira, L.C. de Souza, K.M.S. Dalago, and A. Andrade, "Clinical applicability of infrared thermography in rheumatic diseases: A systematic review," *J. Therm. Biol.*, vol. 104, p. 103172, Feb. 2022, doi: 10.1016/j.jtherbio.2021.103172.

[37] J. Molenda and A. Charchalis, "Using thermovision for temperature measurements during turning process," *J. KONES.*, vol. 25, no. 4, pp. 293–298, 2018, doi: 10.5604/01.3001.0012.4803.

[38] A. Uhryński and M. Bembenek, "The Thermographic Analysis of the Agglomeration Process in the Roller Press of Pillow-Shaped Briquettes," *Materials*, vol. 15, no. 8, p. 2870, Jan. 2022, doi: 10.3390/ma15082870.

[39] J.E. Seppala and K.D. Migler, "Infrared thermography of welding zones produced by polymer extrusion additive manufacturing," *Addit. Manuf.*, vol. 12, pp. 71–76, Oct. 2016, doi: 10.1016/j.addma.2016.06.007.

[40] B.G. Compton, B.K. Post, C.E. Duty, L. Love, and V. Kunc, "Thermal analysis of additive manufacturing of large-scale thermoplastic polymer composites," *Addit. Manuf.*, vol. 17, pp. 77–86, Oct. 2017, doi: 10.1016/j.addma.2017.07.006.

[41] D.A. Boiko, V.A. Korabelnikova, E.G. Gordeev, and V.P. Ananikov, "Integration of thermal imaging and neural networks for mechanical strength analysis and fracture prediction in 3D-printed plastic parts," *Sci. Rep.*, vol. 12, no. 1, p. 8944, Dec. 2022, doi: 10.1038/s41598-022-12503-y.

[42] S.F. Costa, F.M. Duarte, and J.A. Covas, "Estimation of filament temperature and adhesion development in fused deposition techniques," *J. Mater. Process. Technol.*, vol. 245, pp. 167–179, Jul. 2017, doi: 10.1016/j.jmatprotec.2017.02.026.

[43] "EASY PETG – Filament PET – simple and pleasant 3D printing," *Fiberlogy*. [Online]. Available: https://fiberlogy.com/en/fiberlogy-filaments/easy-pet-g/ (accessed Nov. 07, 2022).

[44] "Overview of materials for PETG Copolyester." *Matweb.* [Online]. Available: https://www.matweb.com/search/datasheet_print.aspx?matguid=4de1c85bb946406a86c52b688e3810d0 (accessed Nov. 07, 2022).